AGU PUBLICATIONS

JGR

Journal of Geophysical Research: Space Physics

RESEARCH ARTICLE
10.1002/2016JA023508

Special Section:
Major Results From the MAVEN Mission to Mars

Nightside ionosphere of Mars: Composition, vertical structure, and variability

Z. Girazian[1], P. R. Mahaffy[1], R. J. Lillis[2], M. Benna[1,3], M. Elrod[1,4], and B. M. Jakosky[5]

[1]NASA Goddard Space Flight Center, Greenbelt, Maryland, USA, [2]Space Sciences Laboratory, University of California, Berkeley, California, USA, [3]CRESST, University of Maryland Baltimore County, Baltimore, Maryland, USA, [4]CRESST, University of Maryland, College Park, Maryland, USA, [5]Laboratory for Atmospheric and Space Physics, University of Colorado Boulder, Boulder, Colorado, USA

Key Points:
- The composition of the nightside ionosphere of Mars is characterized
- O_2^+ is the major nightside ion down to 130 km, below which NO^+ becomes the major ion
- Nightside ion densities can vary by nearly an order of magnitude over monthlong timescales

Correspondence to:
Z. Girazian,
zachary.r.girazian@nasa.gov

Citation:
Girazian, Z., P. R. Mahaffy, R. J. Lillis, M. Benna, M. Elrod, and B. M. Jakosky (2017), Nightside ionosphere of Mars: Composition, vertical structure, and variability, *J. Geophys. Res. Space Physics*, *122*, doi:10.1002/2016JA023508.

Received 26 SEP 2016
Accepted 30 MAR 2017
Accepted article online 7 APR 2017

Abstract We provide an overview of the composition, vertical structure, and variability of the nightside ionosphere of Mars as observed by Mars Atmosphere and Volatile EvolutioN (MAVEN)'s Neutral Gas and Ion Mass Spectrometer (NGIMS) through 19 months of the MAVEN mission. We show that O_2^+ is the most abundant ion down to ~130 km at all nightside solar zenith angles (SZA). However, below 130 km NO^+ is the most abundant ion, and NO^+ densities increase with decreasing altitude down to at least 120 km. We also show how the densities of the major ions decrease with SZA across the terminator. At lower altitudes the O_2^+ and CO_2^+ densities decrease more rapidly with SZA than the NO^+ and HCO^+ densities, which changes the composition of the ionosphere from being primarily O_2^+ on the dayside to being a mixture of O_2^+, NO^+, and HCO^+ on the nightside. These variations are in accord with the expected ion-neutral chemistry, because both NO^+ and HCO^+ have long chemical lifetimes. Additionally, we present median ion density profiles from three different nightside SZA ranges, including deep on the nightside at SZAs greater than 150° and discuss how they compare to particle precipitation models. Finally, we show that nightside ion densities can vary by nearly an order of magnitude over monthlong timescales. The largest nightside densities were observed at high northern latitudes during winter and coincided with a major solar energetic particle event.

1. Introduction

In the 1970s the Viking Landers obtained the first in situ observations of the dayside ionosphere of Mars. These observations showed that the dayside ionosphere is composed primarily of O_2^+ ions and confirmed that photoionization by solar EUV radiation is the primary source of dayside plasma [*Hanson et al.*, 1977; *Chen et al.*, 1978; *Fox et al.*, 1996; *Withers*, 2009]. By contrast, in situ observations of the nightside ionosphere were unavailable until 2014 when the Mars Atmosphere and Volatile EvolutioN (MAVEN) mission arrived at Mars [*Jakosky et al.*, 2015a, 2015b]. Consequently, the composition and sources of the nightside ionosphere are not as well understood.

It has been suggested that there are two main sources of plasma in the upper nightside ionosphere. The first being impact ionization from precipitating particles, which are thought mostly to be electrons of solar wind origin [*Verigin et al.*, 1991; *Fox et al.*, 1993; *Haider*, 1997] but may also include solar wind protons, energetic neutral atoms (ENAs), and dayside photoelectrons [*Kallio and Janhunen*, 2001; *Haider et al.*, 2013; *DiéVal et al.*, 2013; *Xu et al.*, 2016]. The second source of plasma is thought to be day-to-night ion transport driven by cross-terminator winds [*Chaufray et al.*, 2014; *Cui et al.*, 2015]. However, even in the absence of winds ions can be transported to the nightside, as long as the ionosphere and the planet rotate as a solid body and the ions have long chemical lifetimes [*Cui et al.*, 2009; *González-Galindo et al.*, 2013; *Cui et al.*, 2015].

Before MAVEN, constraints on the nightside ionosphere came primarily from remote sensing observations of the electron density and total electron content by radio occultation experiments on the Mars, Viking, and Mars Express missions, and from the MARSIS radar sounding experiment on Mars Express [*Zhang et al.*, 1990; *Mendillo et al.*, 2003; *Gurnett et al.*, 2008; *Duru et al.*, 2011; *Němec et al.*, 2010; *Withers et al.*, 2012; *Cartacci et al.*, 2013; *Diéval et al.*, 2014; *Němec et al.*, 2014; *Cui et al.*, 2015]. These observations have revealed that the nightside ionosphere is patchy and spatially inhomogeneous with peak densities on the order of a few 10^3–10^4 cm^{-3}. They have also shown that nightside densities are larger near regions of vertical crustal magnetic fields [e.g., *Safaeinili et al.*, 2007; *Lillis et al.*, 2011; *Němec et al.*, 2011; *Dubinin et al.*, 2016].

Initial MAVEN observations have provided further constraints on the nightside ionosphere. An analysis of nightside electron density profiles concluded that precipitating energetic electrons are needed to sustain the nightside ionosphere [*Fowler et al.*, 2015]. In addition, observations of electron energy spectra suggest that dayside photoelectrons can be transported across the terminator along closed crustal field loops, then precipitate into the nightside atmosphere [*Xu et al.*, 2016]. This process may be an important nightside ionization source in addition to precipitating electrons of solar wind origin.

Furthermore, the MAVEN Neutral gas and Ion Mass Spectrometer (NGIMS) has provided the first in situ observations of the nightside ion composition. Initial NGIMS observations have shown the general day-to-night variations of several ions and revealed that O_2^+, NO^+, and HCO^+ are the major species in the lower nightside ionosphere [*Benna et al.*, 2015a; *Fox et al.*, 2015]. However, these studies were limited to solar zenith angles less than ~130° and did not focus on the bulk composition of the nightside ionosphere nor its variability.

Our goal in this paper is to describe some of the basic characteristics of the nightside ionosphere by providing an overview of its composition, vertical structure, and variability as observed by NGIMS over the first 19 months of the MAVEN mission. In section 2 we introduce and describe the NGIMS data set; in section 3 we show how the composition of the ionosphere changes from day-to-night across the dawn and dusk terminators; in section 4 we present median ion density profiles from the nightside; in section 5 we show that nightside ion densities from different latitudes and seasons can vary substantially; and in section 6 we summarize our results and present our conclusions.

2. NGIMS Data Description

MAVEN began its nominal science mission in November 2014. The 4.5 h orbit of MAVEN is highly elliptical with an apoapsis of ~6200 km and a periapsis that is typically ~150 km, although there have been several "deep dip" campaigns that lowered the periapsis down to ~125 km for short periods of time [*Jakosky et al.*, 2015b, 2015a]. The periapsis of MAVEN precesses slowly so that the spacecraft latitude, local time, and solar zenith angle (SZA) are similar from orbit to orbit, but vary considerably over the course of the mission. This orbit allows NGIMS to determine the composition of the ionosphere over a wide range of conditions. However, during any single orbit, the spacecraft does not travel vertically (radial direction) through the ionosphere. Since NGIMS observations are made along the spacecraft trajectory, vertical ion density profiles are not measured directly. Instead, vertical profiles can only be derived by averaging observations from several orbits [e.g., *Benna et al.*, 2015a; *Fowler et al.*, 2015; *Withers et al.*, 2015]. The resulting vertical profiles, however, represent averages over time, space, and changing underlying conditions (e.g., magnetic topology).

NGIMS has several observing modes that allow it to measure either neutrals or ions. The observing mode is typically alternated so that ion density measurements are collected every other orbit (9 h apart). Detailed descriptions of the NGIMS instrument, data calibration, and initial scientific results have been presented in several publications [*Benna et al.*, 2015b, 2015a; *Mahaffy et al.*, 2015b, 2015a].

Our analysis uses the Level 2 (v06_r02) NGIMS ion data that were obtained between 18 October 2014 and 30 July 2016. Figure 1 shows the SZA-altitude coverage of the data set along with how the SZA and seasonal coverage have evolved throughout the mission. We adopt the SZA convention such that positive SZAs represent dusk measurements (local times >12 h) and negative SZAs represent dawn measurements (local times <12 h).

We focus on observations near the terminator and extending into the nightside, which we define as observations at SZAs greater than 110°. This definition is somewhat arbitrary but was chosen because at this SZA the thermosphere is shaded from the Sun (blocked by solid Mars) at altitudes up to 220 km. We note that at 300 km the thermosphere does not reach the shaded region until a SZA of 113° and that previous studies have defined the nightside using their own SZA conventions [e.g., *Němec et al.*, 2011; *Withers et al.*, 2012].

The NGIMS data set includes 1210 orbits of ion density measurements, 523 of which include nightside observations below 300 km. These nightside observations were obtained during four different time periods throughout the mission. The different latitudes, seasons, and local times (dawn/dusk) covered during each time period are highlighted in Figure 1 and listed in Table 1.

There is a clear bias in the data set with respect to latitude and season. For example, data from high northern latitudes only cover the winter and fall seasons while data from low southern latitudes only cover spring equinox. Additionally, there is a bias in the data set with respect to dawn and dusk. For example, most of the

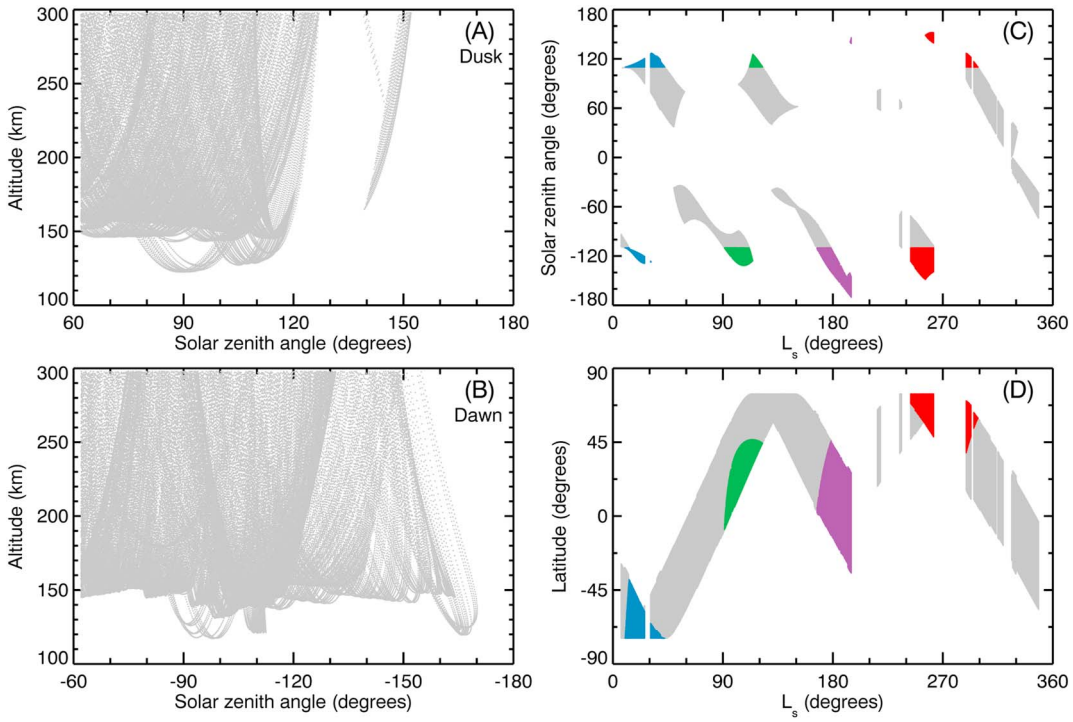

Figure 1. The SZA, altitude, latitude, and solar longitude (L_s) distribution of the NGIMS ion data set. (a) The altitude and SZA distribution of the dusk observations (positive SZAs). (b) The altitude and SZA distribution of the dawn observations (negative SZAs). In these two panels each gray dot shows the location of a NGIMS ion observation. For clarity, only half of the observations are shown. (c) The SZA of the NGIMS ion observations below 300 km as a function of L_s. Gray points show dayside observations and colored points show nightside observations (SZA > 110°). The colors highlight the four different time periods of nightside observations within the data set. The red points are from the first period of observations and the blue, green, and purple points are from the second, third, and fourth periods, respectively. (d) Same as Figure 1c but showing latitude versus L_s.

June/July 2016 observations are from dawn while few are from dusk. These biases must be kept in mind when comparing ion densities from the different time periods. Differences between the subsets of data may be caused by variations in the nightside plasma source or by diurnal and seasonal variations in the composition of the neutral atmosphere. The biases make it difficult to distinguish between these two sources of variability.

As Figure 1 shows, the nightside observations extend to SZAs up to ~170°, but the SZA-altitude distribution of the observations are nonuniform (Figures 1a and 1b), with more observations at dawn than dusk, and fewer observations at SZAs greater than 120°. Only in the most recent period of nightside observations did NGIMS sample the ionosphere at SZAs past 150°. These recent observations included a "deep dip" campaign allowing NGIMS to sample the nightside ionosphere down to 120 km near midnight.

The observations were obtained during the declining phase of Solar Cycle 24, corresponding to moderate and minimum solar conditions. Throughout this period the EUV irradiance at Mars changed by a factor of about 2, primarily owing to the varying Mars-Sun distance rather than solar cycle variability. The EUV irradiance was highest during the beginning of the mission, when Mars was near perihelion [*Bougher et al.*, 2017; *Lee et al.*, 2017].

Table 1. The Four Different Periods of NGIMS Nightside Ion Measurements Used in This Study (SZA > 110°)

Dates (mm/dd/yy)	# Dawn Orbits	# Dusk Orbits	L_s	Latitudes	Season
11/30/2014 to 2/26/2015	61	60	245°–300°	40°N–75°N	Northern winter
7/8/2015 to 9/16/2015	88	141	10°–40°	38°S–74°S	Spring equinox
11/6/2016 to 3/14/2016	133	58	90°–120°	8°S–47°N	Northern summer
6/11/2016 to 7/30/2016	111	4	165°–195°	34°S–45°N	Fall equinox

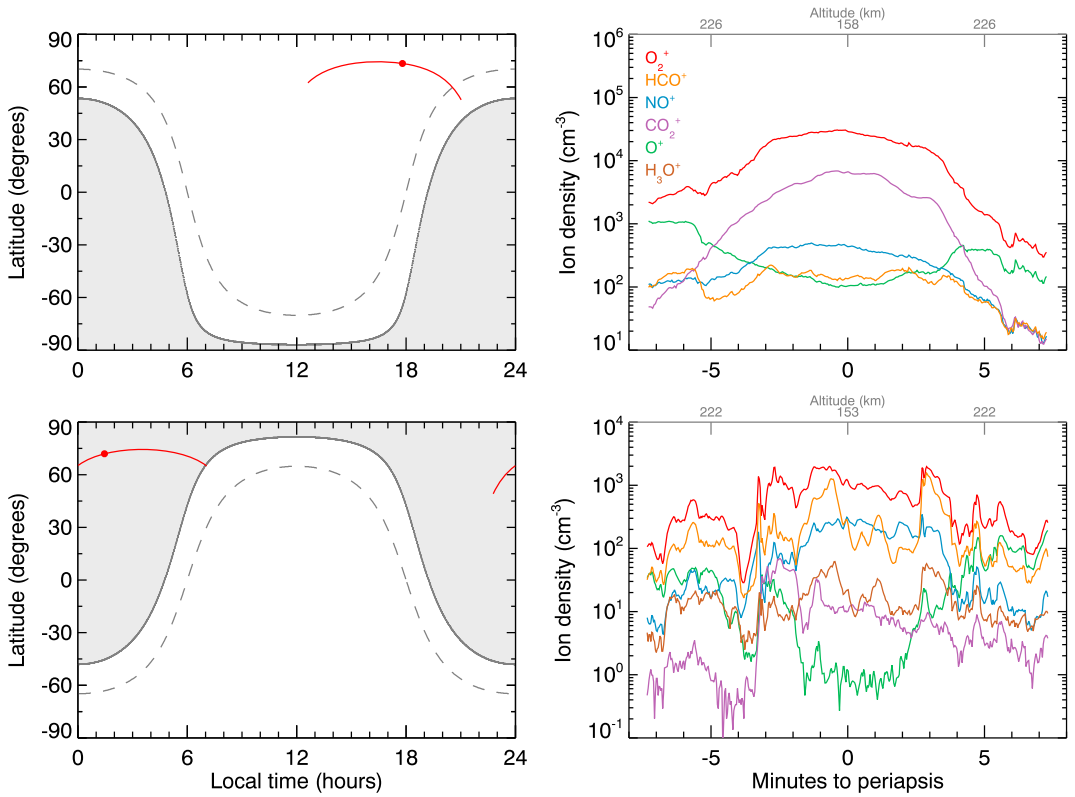

Figure 2. Ion densities measured by NGIMS along (top row) one dayside orbit (orbit 2893) and (bottom row) one nightside orbit (orbit 483). (left column) The red line shows the trajectory of MAVEN through latitude and local time during each orbit and the red dot shows the location of periapsis. The dashed line shows where SZA = 90° and the shaded region identifies the nightside (SZA > 110°). (right column) The measured ion densities as a function of time during the orbits. The top axes in these panels indicate the spacecraft altitude. Note that the H_3O^+ densities are too small to be visible in the dayside panel.

Although the data set includes many ion species, we focus on those that are the most abundant on either the dayside or the nightside. These include O_2^+, CO_2^+, O^+, NO^+, and HCO^+ [*Benna et al.*, 2015a]. We assume that all mass 29 ions are HCO^+ even though they cannot be differentiated from other mass 29 ions such as N_2H^+ and HOC^+. Nevertheless, this is a reasonable assumption because models predict that HCO^+ is by far the most abundant mass 29 ion [*Matta et al.*, 2013; *Fox*, 2015; *Fox et al.*, 2015].

We define the total ion density, N_{tot}, as the sum of the O_2^+, NO^+, CO_2^+, O^+, HCO^+, N_2^+/CO^+, and H_3O^+ densities. This approximation underestimates the true ion density because not every species is included. Nevertheless, it does include the most abundant species on the dayside and the nightside, and results from *Benna et al.* [2015a] suggest that this approximation underestimates the actual total ion density by less than 5%. We also define the relative ion abundance for a given species as the ion density divided by the total ion density and expressed as a percentage.

Figure 2 shows examples of NGIMS ion observations during a single dayside orbit and a single nightside orbit. The spacecraft trajectory through latitude and local time is shown in the left column and the measured O_2^+, CO_2^+, O^+, HCO^+, NO^+, and H_3O^+ densities are shown in the right column. There are some striking differences between the dayside and nightside observations. For example, the dayside ion densities vary smoothly along the spacecraft trajectory but the nightside densities vary substantially, demonstrating the patchy nature of the nightside ionosphere.

In addition to the larger variability on the nightside, there is also a difference in the ion composition at lower altitudes. On the dayside O_2^+ is the dominant ion, CO_2^+ is the second most abundant ion, and NO^+ and HCO^+ are minor components. On the nightside, however, the composition is somewhat different. Although O_2^+ is still the most abundant ion (although not as dominant), CO_2^+ is now a minor ion and HCO^+ and NO^+ are major components. Additionally, H_3O^+ —which is a minor species on dayside—is the fourth most abundant species

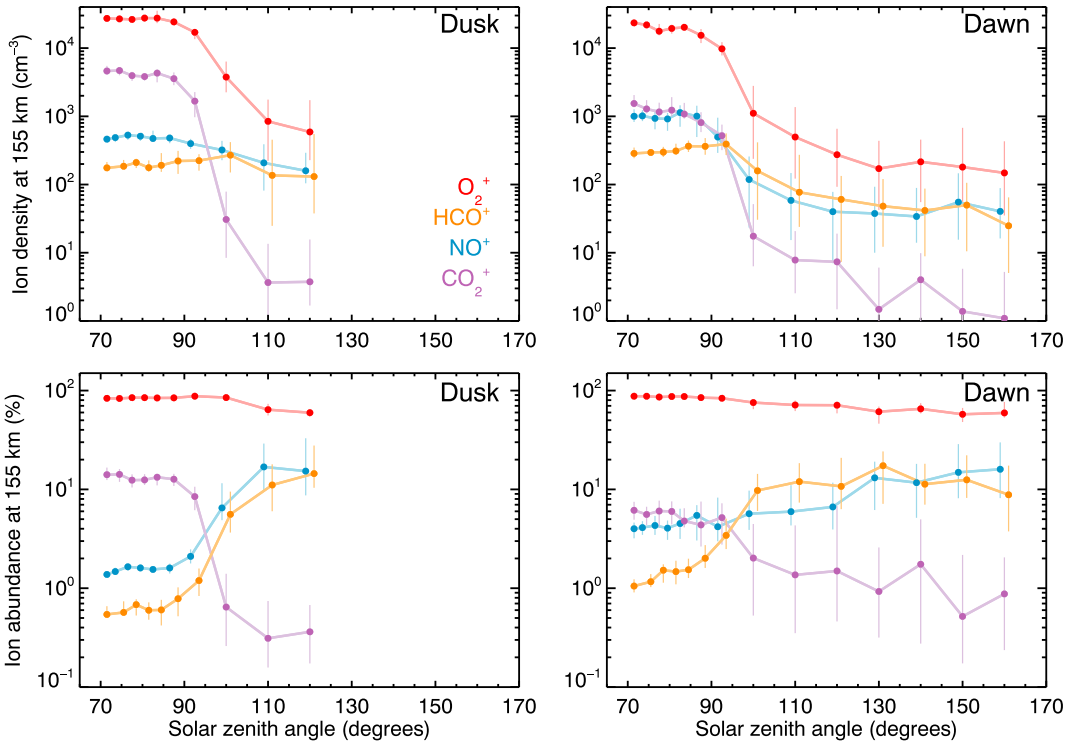

Figure 3. (top row) Median ion densities at 155 km as a function of SZA across the dusk (left) and dawn (right) terminators. (bottom row) The corresponding relative ion abundances at 155 km. In both panels the circles show the median values after binning in SZA, and the error bars show the 25% and 75% quartiles.

on the nightside. However, as Figure 2 demonstrates, its densities are typically 10–100 times smaller than either NO^+ or HCO^+. Therefore, we exclude H_3O^+ in the rest of the paper. A discussion of nightside H_3O^+ and its implications for the presence of water in the thermosphere has been presented by *Fox et al.* [2015].

These observations reveal two major features that distinguish the nightside ionosphere from the dayside ionosphere: larger relative abundances of NO^+ and HCO^+, and enhanced variability. In the sections that follow we will further analyze the data by binning observations from multiple orbits in altitude and SZA to obtain a statistical picture of the nightside composition.

3. Composition

In section 3.1 we show how the ion composition changes across the dawn and dusk terminators and in section 3.2 we interpret the results in terms of ion chemistry. In both sections the results are obtained by averaging data from the four different time periods of nightside observations (Table 1). As discussed in section 3.2, the four periods cover different latitudes and seasons, which may introduce a bias in the results. Nevertheless, the results presented here will provide a broad overview of how the composition changes across the terminator.

3.1. Changes in Ion Composition Across the Dawn and Dusk Terminators

Figure 3 (top left) shows the median O_2^+, HCO^+, NO^+, and CO_2^+ densities, and their 25%/75% quartiles, at 155 (±1) km as a function of SZA across the dusk terminator. This figure includes all the NGIMS ion observations obtained at dusk SZAs greater than +70°.

The CO_2^+ and O_2^+ densities decrease more rapidly with SZA than the NO^+ and HCO^+ densities. As a result, nightside CO_2^+ densities are more than 1000 times smaller than those on the dayside (4.0×10^3 to 0.5×10^0 cm^{-3}) and nightside O_2^+ densities are ~50 times smaller than on the dayside (3.0×10^4 to 6.0×10^2 cm^{-3}). By contrast, nightside NO^+ densities are only ~3 times smaller than on the dayside (5.0×10^2 to 2.0×10^2 cm^{-3}) and nightside HCO^+ densities are comparable to their dayside values ($1.0–2.0 \times 10^2$ cm^{-3}).

Because the four ions have different SZA variations across the terminator, their relative abundances change, leading to a nightside composition that is different than the dayside. This is illustrated in Figure 3 (top right),

which shows the relative ion abundances at 155 km. The most abundant ion at all SZAs is O_2^+, but its relative abundance decreases from ~85% on the dayside to only ~60% on the nightside. Additionally, although CO_2^+ is the second most abundant species on the dayside with a relative abundance of ~15%, its rapid decay across the terminator leads to a nightside relative abundance of less than 1%. Meanwhile, HCO^+ and NO^+—which are minor species on the dayside—become the second and third most abundant species on the nightside with relative abundances between 10 and 20% (NO^+ being slightly more abundant).

The densities and relative abundances are also more variable on the nightside than on the dayside. For example, the interquartile ratios (the interquartile range as a percentage of the median) of the O_2^+ densities increase from 1% on the dayside to over 100% on the nightside. A similar trend is seen in the O_2^+ relative abundances where the interquartile ratio increases from 4% on the dayside to more than 20% on the nightside. Thus, at 155 km the dayside ionosphere has a stable composition that is ~85% O_2^+ ions while the nightside ionosphere has variable composition that is only ~60% O_2^+ ions.

Figure 3 (bottom row) also shows median ion densities and relative abundances at 155 km as a function of SZA across the dawn terminator. We calculated the median values using only measurements from the third and fourth periods of nightside observations. Unlike the dusk observations shown in Figure 3, the dawn observations extend to higher nightside SZAs up to 160°.

The SZA variations across the dawn terminator are similar to those across the dusk terminator with CO_2^+ and O_2^+ decreasing more rapidly with SZA than HCO^+ and NO^+. At SZAs >110° the ion composition at dawn is broadly consistent with the ion composition at dusk with the relative abundance of O_2^+ at ~60% and the relative abundances of HCO^+ and NO^+ between 10 and 20%. There are, however, minor differences in the dawn and dusk ion compositions (e.g., the relative abundance of NO^+ is larger at dusk), but they may be caused by the latitude and seasonal bias in the data set (Table 1) rather than by a true dawn-dusk asymmetry.

On the dayside near the terminator (SZA = 70–90°) there are differences in the ion composition at dawn and dusk. At dawn CO_2^+ densities are 4 times smaller and NO^+ and HCO^+ densities are 2 times larger. This dawn-dusk asymmetry may also be due to the seasonal bias in the data set. However, this asymmetry is predicted by the Laboratoire de Météorologie Dynamique (LMD) Mars General Circulation Model. It is attributed to a dawn-dusk asymmetry in the composition of the neutral atmosphere (e.g., atomic oxygen) driven by cooler temperatures at dawn than at dusk [*González-Galindo et al.*, 2013; *Chaufray et al.*, 2014].

Next we show how the composition changes across the dusk terminator at altitudes between 130 and 300 km. We do so by comparing median ion density profiles from the near-terminator dayside (SZA = +75–80°) to median ion density profiles from the near-terminator nightside (SZA = +110–120°). To construct the density profiles, we separated all the nightside data into the specified SZA ranges and into 12 km altitude bins, then calculated the median ion density within each bin. The median profiles and the ratios between the nightside and dayside profiles are shown in Figure 4.

The density profiles in Figure 4a show that O_2^+ is the most abundant ion at all altitudes near the dayside dusk terminator. Above 200 km the topside is a mixture of O_2^+ and O^+, but below 200 km O^+ becomes a minor species and CO_2^+ becomes the second most abundant ion. Additionally, NO^+ and HCO^+ are minor species at all altitudes. These dayside profiles are consistent with those presented from Viking Lander and early NGIMS observations [*Hanson et al.*, 1977; *Benna et al.*, 2015a; *Withers et al.*, 2015].

The nightside density profiles in Figure 4b show that, like the dayside, O_2^+ is the most abundant ion at all altitudes and the topside is a mixture of O_2^+ and O^+. However, unlike the dayside, CO_2^+ is a minor species below 200 km where the composition is a mixture of O_2^+, HCO^+, and NO^+. There is a peak in the HCO^+ density profile near 155 km with a peak density of 1.2×10^2 cm^{-3}. There is no distinct peak in the O_2^+, NO^+, or N_{tot} density profiles and their maximum densities are at 130 km, the lowest altitude observed. There, the maximum N_{tot} density is 1.7×10^3 cm^{-3}, the maximum O_2^+ density is 8.7×10^2 cm^{-3}, and the maximum NO^+ density is 7.4×10^2 cm^{-3}. Hence, NO^+ is a major ion in the nightside ionosphere and if there is a peak at lower altitudes, it will not be dominated by O_2^+.

The ratios between the night and day profiles in Figure 4c show that the densities of all five species are depleted compared to their dayside values, but the amount in which they are depleted varies with altitude. Above 200 km the night/day ratios of all species, except for CO_2^+, follow similar altitude trends and the nightside densities are 10–250 times smaller than on the dayside. Alternatively, below 200 km there are substantial differences between the day/night ratios of each species. For example, the O_2^+ and CO_2^+ ratios are nearly

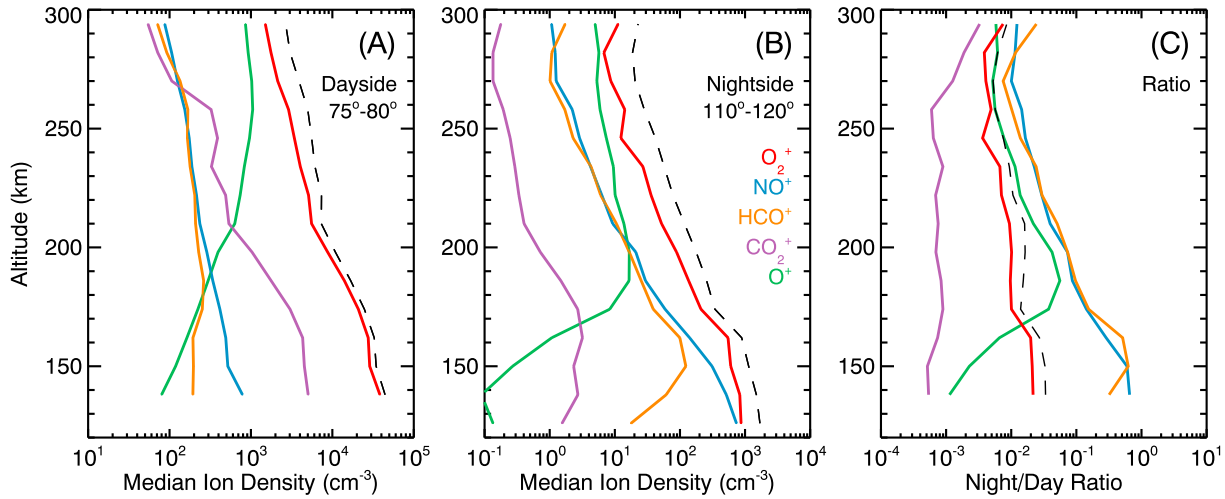

Figure 4. (a) Dayside median density profiles from near the dusk terminator at SZAs between +75° and +80°. The different colors correspond to different ion species, and the dashed line is the total ion density. (b) Same as Figure 4a but showing nightside median density profiles from dusk SZAs between +110° and +120°. (c) The ratios between the nightside and dayside median density profiles, which illustrates how the densities decay across the terminator.

constant with altitude such that the nightside O_2^+ densities are 5–100 times smaller than on the dayside and the nightside CO_2^+ densities are more than 1000 times smaller than on the dayside. Alternatively, the O^+ night/day ratios peak near 180 km then decrease rapidly at lower altitudes. The NO^+ and HCO^+ night/day ratios share similar altitude trends that are different than the other species. Their ratios increase with decreasing altitude and the nightside densities below 180 km are only 1–10 times smaller than on the dayside.

In summary, the ion densities decrease across the terminator with the largest variations occurring between SZAs 85°–100°, the region where EUV radiation diminishes rapidly and photoionization can no longer sustain the ionosphere. The O_2^+ and CO_2^+ densities decrease more rapidly across the terminator than the NO^+ and HCO^+ densities, especially at altitudes below 180 km. This causes the composition below 180 km to change from one that is primarily O_2^+ on the dayside to one that is a variable mixture of O_2^+, NO^+, and HCO^+ on the nightside.

3.2. Ion Chemistry and Chemical Lifetimes

The different density variations across the terminator for each ion species can be interpreted in terms of ion chemistry, which controls each species' chemical lifetime and its ability to survive across the terminator [e.g., *Cui et al.*, 2009; *González-Galindo et al.*, 2013; *Fox et al.*, 2015]. In general, ions that are lost through reactions with neutrals will have short chemical lifetimes and ions lost through dissociative recombination (DR) with an electron will have long chemical lifetimes [*Cui et al.*, 2009].

The rapid decay of CO_2^+ across the terminator suggests that it has a short chemical lifetime, which is consistent with model predictions [*Fox et al.*, 1993; *Haider*, 1997; *González-Galindo et al.*, 2013; *Chaufray et al.*, 2014; *Fox*, 2015]. The chemical lifetime of CO_2^+ is short, because it is quickly destroyed by reactions with atomic oxygen that convert it into O^+ and O_2^+, and a reaction with H_2 that converts it into $OCOH^+$. Thus, at SZAs near the terminator and on the nightside where EUV radiation is diminished, there is no longer a photoionization source to replenish the CO_2^+ ions and they quickly become a minor species.

The slow decay of NO^+ and HCO^+ suggests that these ions have long chemical lifetimes, which is also consistent with model predictions [*Haider*, 1997; *Krasnopolsky*, 2002; *González-Galindo et al.*, 2013; *Matta et al.*, 2013; *Chaufray et al.*, 2014; *Fox et al.*, 2015; *Fox*, 2015]. Both NO^+ and HCO^+ are predicted to be terminal ions with long chemical lifetimes, because they are produced by several ion-neutral reactions, but destroyed mainly through DR. NO^+ is a terminal ion, because it has a low ionization potential, it has two major production sources [*Haider*, 1997; *González-Galindo et al.*, 2013]:

$$O_2^+ + N \rightarrow NO^+ + O \quad (1)$$

$$O_2^+ + NO \rightarrow NO^+ + O_2 \quad (2)$$

Table 2. Estimates of the Chemical Lifetimes of Several Species in the Nightside Ionosphere at 155 km and SZA > 130°[a]

Species	Density (10^2 cm^{-3})	DR Coefficient (cm^3 s^{-1})	Chemical Lifetime (h)
NO^+	0.5	$4.0 \times 10^{-7}(300/T_e)^{0.5}$	3.0
HCO^+	0.5	$2.0 \times 10^{-7}(300/T_e)^{1.25}$	2.5
O_2^+	2.0	$2.4 \times 10^{-7}(300/T_e)^{0.7}$	2.7
e^-	3.0		2.7

[a]For each species in column 1, column 2 lists its typical density at 155 km, column 3 its dissociative recombination (DR) coefficient, and column 4 its chemical lifetime. The lifetime for O_2^+ is an upper limit (see text). The DR coefficient for HCO^+ is from *Fox* [2015] and the others from *Schunk and Nagy* [2009]. We have adopted a value of $T_e = 500$ K based on *Fowler et al.* [2015].

The larger night/day ratios of NO^+ below 180 km (Figure 4) are consistent with these production sources because at lower altitudes, O_2^+, NO, and N densities are larger, making reactions (1) and (2) more efficient. Thus, the decay of NO^+ across the terminator is slow because O_2^+ is continuously being converted into NO^+ through reactions (1) and (2). This behavior is also consistent with the LMD general circulation model, which predicts that NO^+ is a major component of the lower nightside ionosphere, even in the absence of electron precipitation or winds [*González-Galindo et al.*, 2013; *Chaufray et al.*, 2014].

HCO^+ is a terminal ion because its parent neutral, CO, has a large proton affinity. It is produced by several ion-neutral reactions, all of which involve hydrogen-bearing neutral or ion species [*Krasnopolsky*, 2002; *Matta et al.*, 2013; *Fox et al.*, 2015; *Fox*, 2015]. Like NO^+, the HCO^+ night/day ratios are larger at lower altitudes, suggesting that ion-neutral reactions are a production source on the nightside. However, unlike NO^+, the HCO^+ nightside density profile and night/day ratios peak near 150 km and drop off rapidly below. This may indicate an additional HCO^+ loss process that becomes important below 150 km such as an ion-neutral reaction with atomic carbon [*Fox*, 2015].

The moderate decay of O_2^+ across the terminator suggests that it has a chemical lifetime that is longer CO_2^+ but shorter than NO^+ or HCO^+, which is also consistent with model predictions [*Haider*, 1997; *González-Galindo et al.*, 2013; *Chaufray et al.*, 2014; *Fox et al.*, 2015]. The two major production sources of O_2^+ are [*Haider*, 1997; *Schunk and Nagy*, 2009]

$$CO_2^+ + O \rightarrow O_2^+ + CO \quad (3)$$

$$O^+ + CO_2 \rightarrow O_2^+ + CO \quad (4)$$

The total production rate of O_2^+ then is proportional to the CO_2^+ and O^+ densities. But on the nightside below 180 km, the CO_2^+ and O^+ densities are less than 5.0×10^0 cm^{-3} (Figure 4) and chemical production of O_2^+ should be minor. Without a chemical production source, O_2^+ should decrease steadily throughout the night as it is converted into NO^+ and lost through DR [*González-Galindo et al.*, 2013; *Chaufray et al.*, 2014; *Fox et al.*, 2015]. However, Figure 3 shows that O_2^+ densities at 155 km are nearly constant at SZAs between 130° and 160° and are also larger than NO^+ densities. This suggests that there is a source that replenishes nightside O_2^+ or that O_2^+ has a long chemical lifetime.

We can estimate the chemical lifetimes of species that are lost primarily through DR. These include NO^+, HCO^+, and electrons. The chemical lifetimes, summarized in Table 2, were estimated using $t_i = N_i/L_i$, where t_i is the lifetime, N_i is the ion density, and L_i is the total loss rate [*Cravens et al.*, 2009; *Fox*, 2009; *Cui et al.*, 2009]. For NO^+ and HCO^+ the total loss rate is given by $L_i = \alpha_i N_i N_e$, where α_i is the DR coefficient listed in Table 2. For electrons, the total loss rate is the sum of the O_2^+, NO^+, and HCO^+ DR loss rates. To calculate each lifetime we have adopted typical nightside values of electron and ion densities at 155 km and SZAs >130° (Figure 3). The typical values are listed in Table 2. Additionally, we have adopted a fixed electron temperature of $T_e = 500$ K [*Fowler et al.*, 2015].

The chemical lifetimes of NO^+ and HCO^+ are both nearly 3 h. Their long lifetimes suggest that they may be remnants of plasma produced on the dayside rather than a product of electron precipitation or ion winds. If the ionosphere rotates as a solid body with the planet, then the source of nightside NO^+ and HCO^+ would

be the survival of dayside NO^+ and HCO^+ with additional production from the chemical conversion of dayside CO_2^+ and O_2^+ (from equations (1) and (2)). For NO^+, this is consistent with predictions from the LMD general circulation model [*González-Galindo et al.*, 2013].

Table 2 also includes an estimate of the O_2^+ chemical lifetime which is nearly 3 h. This, however, is an upper limit because it assumes that O_2^+ is lost only through DR and not through ion-neutral reactions with N and NO (equations (1) and (2)). Since the NGIMS nightside measurements of N and NO are not fully calibrated, we cannot present them here. Nevertheless, we can consider the amount of N or NO needed to significantly reduce the lifetime of O_2^+.

The O_2^+ loss rate due to reaction (1) or (2) is given by $L_i = k_i N_i n_i$ where k_i is the rate constant, which is on the order of 10^{-10} ($cm^3\ s^{-1}$) [*Schunk and Nagy*, 2009], and n_i is the neutral density of either N or NO. For the timescale of this loss process to be 3 h, the N or NO density at 155 km would need to be on the order of $10^6\ cm^{-3}$, which is close to the predicted dayside values at this altitude [*Fox*, 1993, 2015]. However, nightside N and NO densities may differ significantly than those on the dayside.

What N or NO density is required for the O_2^+ ion-neutral loss rate to be comparable to the O_2^+ DR loss rate? This threshold density for N or NO can be estimated by equating the O_2^+ DR lifetime to the O_2^+ ion-neutral lifetime, which gives $n_{thresh} \approx 10^3 N_e$. Thus, if N or NO densities exceed the electron density by a factor of 10^3 at a given altitude, then both DR and ion-neutral loss of O_2^+ will be important. In such a scenario the chemical lifetime of O_2^+ would be cut in half compared to its lifetime due to DR only. At 155 km, the O_2^+ lifetime would be on the order of an hour. If N or NO densities exceed the electron density by an even greater factor of 10^4, then DR loss of O_2^+ would be negligible compared to ion-neutral loss. In that scenario the chemical lifetime of O_2^+ would be 10 times shorter than the lifetime due to DR only. At 155 km the lifetime of O_2^+ would only be several minutes.

Hence, without measurements of nightside N or NO we cannot be conclusive about the source of nightside O_2^+ at large SZAs. If nightside N and NO densities are small, then the source of O_2^+ may be the survival of dayside O_2^+ with additional production from the chemical conversion of dayside O^+ and CO_2^+ (from equations (3) and (4)). Alternatively, if nightside N and NO densities are large, then O_2^+ densities must be replenished more readily to survive at such large SZAs. This would require a source such as particle precipitation or day-to-night ion winds.

4. Vertical Structure

In this section we present median ion density profiles from three different nightside SZA ranges and compare them to predictions from electron precipitation models. The SZA ranges include near the dusk terminator at SZAs between +110° and +120°, near the dawn terminator at SZAs between −110° and −120°, and near midnight at SZAs between −150° and −170°. In all three cases the median densities were calculated using 6 km altitude bins. The dawn and dusk profiles were constructed using all the data within the given SZA ranges. The midnight profiles were constructed using data from 38 orbits during the fourth set of nightside observations, which included the first NGIMS observations of the nightside composition at SZAs past 155°. These midnight observations were obtained at equatorial latitudes between −20° and +20°. The median density profiles for all three cases are shown in Figure 5.

The vertical structure of the density profiles are similar in all three cases. At high altitudes the topside densities decrease exponentially with altitude, but at lower altitudes there are broad peaks in the profiles of all species except for NO^+. The O^+ profile peaks near 200 km while the CO_2^+ profile peaks lower between 150 and 160 km. The O_2^+ and HCO^+ profiles peak even lower altitudes between 130 and 150 km, although the O_2^+ peak is not distinct in the dusk or midnight profiles.

In all three cases the NO^+ density profiles have no peak and continue to increase at lower altitudes down to 120 km, which was the lowest altitude observed. In the midnight and dawn profiles the NO^+ density becomes larger than the O_2^+ density between 130 and 140 km. In the dusk profile, NO^+ never overtakes O_2^+, but near 120 km their densities are nearly equal and the trend suggests that NO^+ overtakes O_2^+ at a lower altitude.

As mentioned in section 3.2, the LMD General Circulation model predicts that NO^+ is a major component of the lower nightside ionosphere, even in the absence of electron precipitation or winds [*González-Galindo et al.*, 2013; *Chaufray et al.*, 2014]. In the model the source of the nightside NO^+ is survival of dayside NO^+ and the chemical conversion of dayside CO_2^+ and O_2^+ (equations (1) and (2)).

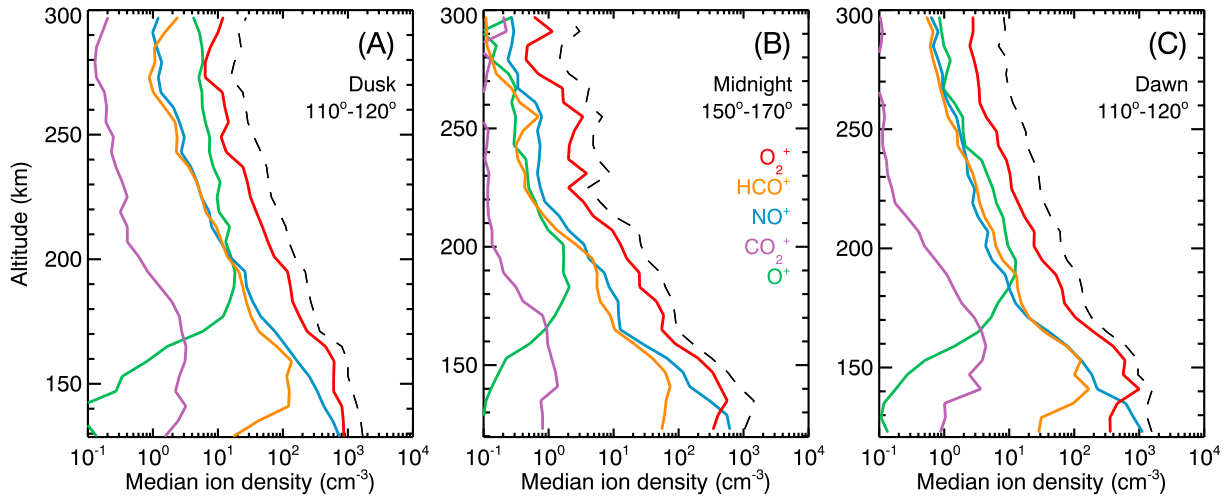

Figure 5. Nightside median density profiles from dawn, dusk, and near midnight. The different colors represent different ion species and the dashed line is the total ion density. (a) Dusk SZAs between +110° and +120°. (b) Near-midnight SZAs between −150° and −170°. (c) Dawn SZAs between −110° and −120°.

Now we discuss how these median density profiles compare to predictions from particle precipitation models. We caution that a direct comparison is limited because our median profiles are derived from observations that cover all longitudes and several latitudes over long periods of time. Thus, they represent temporal and spatial averages over which the precipitation source may vary significantly. Particle precipitation models, however, are often based on single events during which one particle energy spectrum is injected into the atmosphere [e.g., *Fox et al.*, 1993; *Haider*, 1997] or based on particle energy spectra averaged over long periods of time [e.g., *Lillis et al.*, 2011]. Moreover, the energy spectra and neutral atmospheres used in the models may differ from the conditions during the NGIMS observations. Nevertheless, we wish only to compare the major features.

Electron precipitation models predict peaks in the O_2^+ and N_{tot} density profiles between 140 and 180 km, below which the densities decrease rapidly toward lower altitudes [*Fox et al.*, 1993; *Haider*, 1997; *Fillingim et al.*, 2007; *Lillis et al.*, 2009, 2011; *Haider et al.*, 2013]. These peaks are not distinct in our median profiles. However, our detection of the peak is limited due to the spatial and temporal averaging and because most of the NGIMS observations are from altitudes at and above 150 km where the peak is expected to be. Nevertheless, the O_2^+ profiles do appear to have broad peaks in the predicted altitude range suggesting at least some consistency between the predictions and the observations.

Precipitation models also predict peak CO_2^+ densities on the order of 10^2 cm^{-3} near 150 km [*Fox et al.*, 1993; *Haider*, 1997; *Haider et al.*, 2013]. This peak is observed as a broad feature in our median profiles but the peak densities are smaller, on the order of a few 10^0 cm^{-3}. The small CO_2^+ peak densities are partly due to our use of medians rather than averages. For example, at 155 km the median CO_2^+ density at midnight is $\sim 10^0$ cm^{-3} but the average is $\sim 10^1$ cm^{-3}. Although the average is larger than the median, it is still an order of magnitude smaller than predicted by precipitation models. Such small nightside CO_2^+ densities may suggest that particle precipitation is sporadic.

Electron precipitation models also predict a peak in the NO^+ density profile between 130–150 km [*Fox et al.*, 1993; *Haider*, 1997; *Haider et al.*, 2013]. This peak is absent in our median density profiles where NO^+ densities increase with decreasing altitude down to at least 120 km. Taken as a whole, electron precipitation models fail to predict this behavior, which may suggest that the major source of nightside NO^+ is day-to-night transport.

Precipitation models can still be improved as they typically assume chemical equilibrium and neglect vertical diffusion and transport processes which may be important at these altitudes on the nightside. Precipitation models that include improved constraints based on MAVEN data will be useful for investigating the extent in which particle precipitation can explain the composition of the nightside ionosphere.

5. Variability

In this section we show that the nightside ionosphere can vary substantially at different latitudes and seasons. We begin by comparing median ion density profiles from the first and fourth periods of observations.

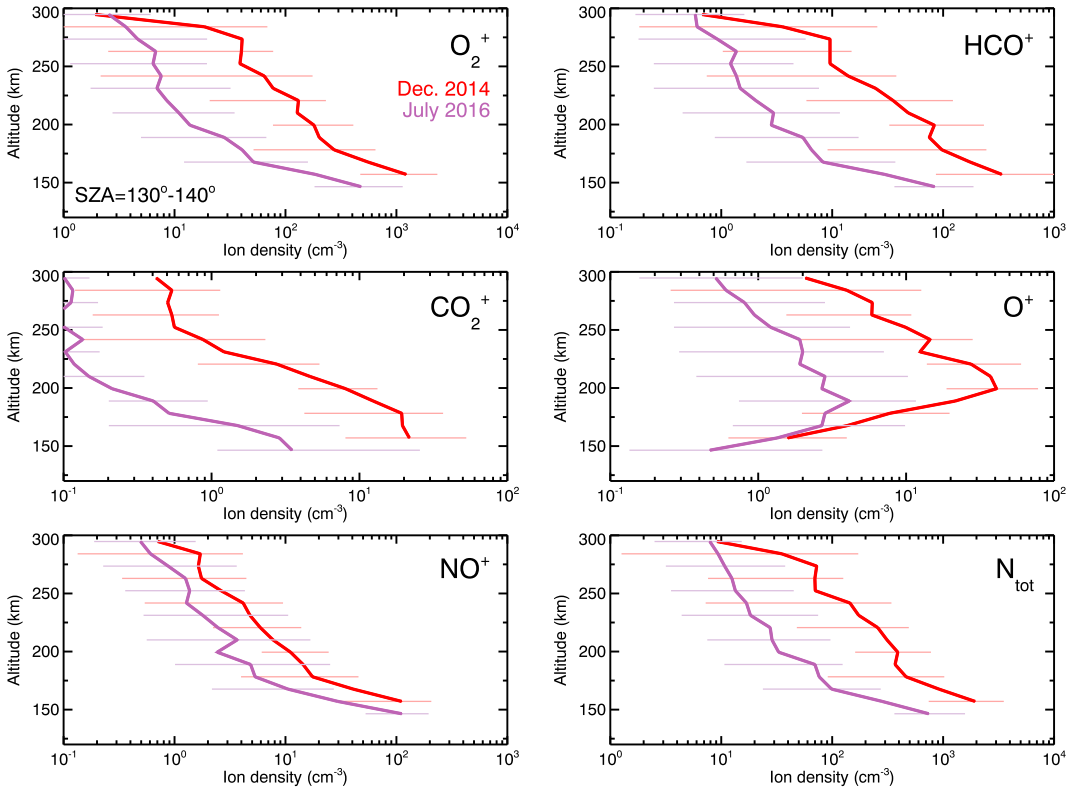

Figure 6. A comparison of the Median ion densities profiles from SZAs −130° to −140° during two different periods of nightside observations. The red density profiles are from December 2014 at high northern latitudes. The purple density profiles are from July 2016 at equatorial latitudes. The error bars show the 25% and 75% quartiles.

These periods were chosen because they contain the only measurements made well into the nightside at SZAs greater than 130°. The first set of observations is from high northern latitudes (+60° to +75°) during winter and the second set is from equatorial latitudes (−10° to +30°) during spring equinox (Table 1).

To construct the median density profiles, we grouped the data by observation period, keeping only data with SZAs between −130° and −140° to ensure that the altitude-SZA distribution of the two periods were similar. Then we separated the data into 10 km altitude bins and calculated the O_2^+, HCO^+, NO^+, CO_2^+, O^+, and N_{tot} median densities, as well as the 25%/75% quartiles within each bin. The median density profiles are shown in Figure 6.

The vertical structure of each density profile is similar during both periods of observations, but during the first period the densities are several times larger (red). The total ion densities and O_2^+ densities are ~8 times larger, the HCO^+ densities are ~15 times larger, and the O^+ peak density is ~10 times larger. The CO_2^+ densities are 10–40 times larger and, interestingly, NO^+ densities are only ~3 times larger.

There are several possibilities for the larger nightside densities during the first period of observations. During this period the solar EUV irradiance was largest, which may indicate that nightside densities increase with increasing solar activity. Another possibility is that the higher densities are due to polar warming. The first period of observations are from high northern latitudes during winter. Northern polar temperatures are warmer during this season as a result of enhanced interhemispheric circulation [*Bougher et al.*, 2006; *Bell et al.*, 2007; *González-Galindo et al.*, 2009; *Bougher et al.*, 2015]. This enhanced circulation may increase the efficiency of day-to-night ion transport resulting in larger nightside densities.

Alternatively, a more plausible explanation may be that the larger nightside densities were the result of a period of enhanced particle precipitation. The first period of observations covered the full month of December 2014, during which the MAVEN Solar Energetic Particle (SEP) instrument [*Larson et al.*, 2015] detected an extended event of energetic electron fluxes [*Lee et al.*, 2017]. These energetic electrons are expected to produce significant ionization at these altitudes [e.g., *Sheel et al.*, 2012] and MARSIS observations show that

nightside densities are enhanced during SEP events [*Němec et al.*, 2014]. This SEP event also produced the so-called "Christmas Lights" aurora event in the northern hemisphere [*Schneider et al.*, 2015].

As our goal here is to characterize the major features in the nightside ionosphere, we refrain from detailed modeling of the nightside ionosphere during such a SEP event. Nevertheless, we have shown that the median nightside ion densities from monthlong time periods at different latitudes and seasons can vary by nearly an order of magnitude. Additionally, the density variations are not uniform by species. In particular, the NO^+ densities are only a factor of ~3 larger during the first period of observations, which is smaller than all other species. Such a small change in the NO^+ may be related to variations in neutral N and NO densities since the main source of NO^+ is through ion-neutral reactions between O_2^+, N, and NO (equations (1) and (2)).

6. Summary and Conclusions

Using in situ observations from the MAVEN Neutral Gas and Ion Mass Spectrometer we have characterized the composition, vertical structure, and variability of the nightside ionosphere of Mars. We showed that below 200 km the SZA variations of CO_2^+ and O_2^+ across the terminator are more rapid than those of NO^+ and HCO^+, which changes the composition from one that is primarily O_2^+ on the dayside to one that is a variable mixture of O_2^+, NO^+, and HCO^+ on the nightside. This change in the composition is driven by ion-neutral chemistry, which—in the absence of a strong and continuous photoionization source—increases the relative abundances of species with long chemical lifetimes. In the ionosphere of Mars these species are NO^+ and HCO^+.

The composition of the nightside ionosphere is more of a mixture of ions than on the dayside, where below 200 km O_2^+ is the dominant species with a relative abundance of at least ~80%. On the nightside above 150 km, however, the relative abundance of O_2^+ is only ~60%. Furthermore, on the nightside below ~130 km, NO^+ overtakes O_2^+ as the most abundant species. Thus, the assumption that the O_2^+ density is equal to the electron density—which is often employed to simplify calculations—is not justified in the lower nightside ionosphere.

The densities of O_2^+ are sustained long into the night which may indicate that O_2^+ is replenished through transport or precipitation. However, the rate at which O_2^+ needs to be replenished to sustain these densities depends critically on the amount of N and NO in the nightside thermosphere, both of which are poorly constrained by observations. This is because the rate at which O_2^+ is converted into NO^+ is proportional to the N and NO densities (equations (1) and (2)). Future constraints on nightside N and NO will be useful for determining the extent in which particle precipitation and day-to-night ion transport supply the nightside ionosphere with O_2^+.

The vertical structure of the nightside ionosphere is somewhat consistent with predictions from electron precipitation models. However, the observations show that the NO^+ density increases with decreasing altitude down to at least 120 km. This behavior presents a challenge to particle precipitation models which predict that the NO^+ density should peak at higher altitudes and decrease rapidly below [e.g., *Fox et al.*, 1993; *Haider*, 1997; *Fillingim et al.*, 2007; *Haider et al.*, 2013]. Large NO^+ densities in the lower nightside ionosphere are predicted, however, by the LMD general circulation model, even without precipitation or winds [*González-Galindo et al.*, 2013; *Chaufray et al.*, 2014]. This suggests that NO^+, which has a chemical lifetime of several hours, may be easily transported from the dayside.

We have also shown that nightside ion densities vary by nearly an order of magnitude over small time and spatial scales as well as over monthlong periods. Densities were largest at high northern latitudes during northern winter. Such large densities may be caused by enhanced day-to-night ion circulation associated with polar warming or enhanced electron precipitation due to an extended solar energetic particle event during that time.

In summary, the enhanced relative abundances of NO^+ and HCO^+ in the nightside ionosphere are consistent with our knowledge of the ion-neutral chemistry at Mars. However, the contributions from the different nightside ion sources—particle precipitation, day-to-night ion winds, and the chemical survival of dayside plasma—need to be constrained in more detail. Such a task will become attainable as MAVEN continues to monitor the nightside ionosphere under different conditions. Continued monitoring will also be useful for exploring the drivers of the nightside variability which may be linked to crustal magnetic field conditions, ion circulation patterns, thermospheric conditions, and changes in the energetic particle environment.

Acknowledgments
Z.G.'s research was supported by an appointment to the NASA Postdoctoral Program at the NASA Goddard Space Flight Center, administered by Universities Space Research Association under contract with NASA. The authors thank Joe Grebowsky for useful discussions and Vladimir Krasnopolsky and an annonymous reviewer for improving the paper. The data used in this publication are publicly available and can be downloaded from the Planetary Data System (http://atmos.nmsu.edu/PDS/data/PDS4/MAVEN/ngims_bundle/l2/).

References

Bell, J. M., S. W. Bougher, and J. R. Murphy (2007), Vertical dust mixing and the interannual variations in the Mars thermosphere, *J. Geophys. Res.*, *112*, E12002, doi:10.1029/2006JE002856.

Benna, M., P. R. Mahaffy, J. M. Grebowsky, J. L. Fox, R. V. Yelle, and B. M. Jakosky (2015a), First measurements of composition and dynamics of the Martian ionosphere by MAVEN's Neutral Gas and Ion Mass Spectrometer, *Geophys. Res. Lett.*, *42*, 8958–8965, doi:10.1002/2015GL066146.

Benna, M., P. R. Mahaffy, J. M. Grebowsky, J. M. C. Plane, R. V. Yelle, and B. M. Jakosky (2015b), Metallic ions in the upper atmosphere of Mars from the passage of comet C/2013 A1 (Siding Spring), *Geophys. Res. Lett.*, *42*, 4670–4675, doi:10.1002/2015GL064159.

Bougher, S. W., J. M. Bell, J. R. Murphy, M. A. Lopez-Valverde, and P. G. Withers (2006), Polar warming in the Mars thermosphere: Seasonal variations owing to changing insolation and dust distributions, *Geophys. Res. Lett.*, *33*, L02203, doi:10.1029/2005GL024059.

Bougher, S. W., D. Pawlowski, J. M. Bell, S. Nelli, T. McDunn, J. R. Murphy, M. Chizek, and A. Ridley (2015), Mars global ionosphere-thermosphere model: Solar cycle, seasonal, and diurnal variations of the Mars upper atmosphere, *J. Geophys. Res.*, *120*, 311–342, doi:10.1002/2014JE004715.

Bougher, S. W., et al. (2017), The structure and variability of Mars dayside thermosphere from MAVEN NGIMS and IUVS measurements: Seasonal and solar activity trends in scale heights and temperatures, *J. Geophys. Res.*, *122*(1), 1296–1313, doi:10.1002/2016JA023454.

Cartacci, M., E. Amata, A. Cicchetti, R. Noschese, S. Giuppi, B. Langlais, A. Frigeri, R. Orosei, and G. Picardi (2013), Mars ionosphere total electron content analysis from MARSIS subsurface data, *Icarus*, *223*, 423–437, doi:10.1016/j.icarus.2012.12.011.

Chaufray, J.-Y., F. Gonzalez-Galindo, F. Forget, M. Lopez-Valverde, F. Leblanc, R. Modolo, S. Hess, M. Yagi, P.-L. Blelly, and O. Witasse (2014), Three-dimensional Martian ionosphere model: II. Effect of transport processes due to pressure gradients, *J. Geophys. Res. Planets*, *119*, 1614–1636, doi:10.1002/2013JE004551.

Chen, R. H., T. E. Cravens, and A. F. Nagy (1978), The Martian ionosphere in light of the Viking observations, *J. Geophys. Res.*, *83*, 3871–3876, doi:10.1029/JA083iA08p03871.

Cravens, T. E., et al. (2009), Model-data comparisons for Titan's nightside ionosphere, *Icarus*, *199*, 174–188, doi:10.1016/j.icarus.2008.09.005.

Cui, J., M. Galand, R. V. Yelle, V. Vuitton, J.-E. Wahlund, P. P. Lavvas, I. C. F. Müller-Wodarg, T. E. Cravens, W. T. Kasprzak, and J. H. Waite (2009), Diurnal variations of Titan's ionosphere, *J. Geophys. Res.*, *114*, A06310, doi:10.1029/2009JA014228.

Cui, J., M. Galand, R. V. Yelle, Y. Wei, and S.-J. Zhang (2015), Day-to-night transport in the Martian ionosphere: Implications from total electron content measurements, *J. Geophys. Res. Space Physics*, *120*, 2333–2346, doi:10.1002/2014JA020788.

DiéVal, C., G. Stenberg, H. Nilsson, and S. Barabash (2013), A statistical study of proton precipitation onto the Martian upper atmosphere: Mars Express observations, *J. Geophys. Res. Space Physics*, *118*, 1972–1983, doi:10.1002/jgra.50229.

Diéval, C., D. D. Morgan, F. Němec, and D. A. Gurnett (2014), MARSIS observations of the Martian nightside ionosphere dependence on solar wind conditions, *J. Geophys. Res. Space Physics*, *119*, 4077–4093, doi:10.1002/2014JA019788.

Dubinin, E., M. Fraenz, D. Andrews, and D. Morgan (2016), Martian ionosphere observed by Mars Express. 1. Influence of the crustal magnetic fields, *Planet. Space Sci.*, *124*, 62–75, doi:10.1016/j.pss.2016.02.004.

Duru, F., D. A. Gurnett, D. D. Morgan, J. D. Winningham, R. A. Frahm, and A. F. Nagy (2011), Nightside ionosphere of Mars studied with local electron densities: A general overview and electron density depressions, *J. Geophys. Res.*, *116*, A10316, doi:10.1029/2011JA016835.

Fillingim, M. O., L. M. Peticolas, R. J. Lillis, D. A. Brain, J. S. Halekas, D. L. Mitchell, R. P. Lin, D. Lummerzheim, S. W. Bougher, and D. L. Kirchner (2007), Model calculations of electron precipitation induced ionization patches on the nightside of Mars, *Geophys. Res. Lett.*, *34*, L12101, doi:10.1029/2007GL029986.

Fowler, C. M., et al. (2015), The first in situ electron temperature and density measurements of the Martian nightside ionosphere, *Geophys. Res. Lett.*, *42*, 8854–8861, doi:10.1002/2015GL065267.

Fox, J. L. (1993), The production and escape of nitrogen atoms on Mars, *J. Geophys, Res.*, *98*, 3297–3310, doi:10.1029/92JE02289.

Fox, J. L. (2009), Morphology of the dayside ionosphere of Mars: Implications for ion outflows, *J. Geophys. Res.*, *114*, E12005, doi:10.1029/2009JE003432.

Fox, J. L. (2015), The chemistry of protonated species in the Martian ionosphere, *Icarus*, *252*, 366–392, doi:10.1016/j.icarus.2015.01.010.

Fox, J. L., J. F. Brannon, and H. S. Porter (1993), Upper limits to the nightside ionosphere of Mars, *Geophys. Res. Lett.*, *20*, 1339–1342, doi:10.1029/93GL01349.

Fox, J. L., P. Zhou, and S. W. Bougher (1996), The Martian thermosphere/ionosphere at high and low solar activities, *Adv. Space Res.*, *17*, 203–218, doi:10.1016/0273-1177(95)00751-Y.

Fox, J. L., M. Benna, P. R. Mahaffy, and B. M. Jakosky (2015), Water and water ions in the Martian thermosphere/ionosphere, *Geophys. Res. Lett.*, *42*, 8977–8985, doi:10.1002/2015GL065465.

González-Galindo, F., F. Forget, M. A. López-Valverde, and M. Angelats i Coll (2009), A ground-to-exosphere Martian general circulation model: 2. Atmosphere during solstice conditions—Thermospheric polar warming, *J. Geophys. Res.*, *114*, E08004, doi:10.1029/2008JE003277.

González-Galindo, F., J.-Y. Chaufray, M. A. López-Valverde, G. Gilli, F. Forget, F. Leblanc, R. Modolo, S. Hess, and M. Yagi (2013), Three-dimensional Martian ionosphere model: I. The photochemical ionosphere below 180 km, *J. Geophys. Res.*, *118*, 2105–2123, doi:10.1002/jgre.20150.

Gurnett, D. A., et al. (2008), An overview of radar soundings of the Martian ionosphere from the Mars Express spacecraft, *Adv. Space Res.*, *41*, 1335–1346, doi:10.1016/j.asr.2007.01.062.

Haider, S. A. (1997), Chemistry of the nightside ionosphere of Mars, *J. Geophys. Res.*, *102*, 407–416, doi:10.1029/96JA02353.

Haider, S. A., B. M. Pandya, and G. J. Molina-Cuberos (2013), Nighttime ionosphere caused by meteoroid ablation and solar wind electron-proton-hydrogen impact on Mars: MEX observation and modeling, *J. Geophys. Res. Space Physics*, *118*, 6786–6794, doi:10.1002/jgra.50590.

Hanson, W. B., S. Sanatani, and D. R. Zuccaro (1977), The Martian ionosphere as observed by the Viking Retarding Potential Analyzers, *J. Geophys. Res.*, *82*, 4351–4363, doi:10.1029/JS082i028p04351.

Jakosky, B. M., J. M. Grebowsky, J. G. Luhmann, and D. A. Brain (2015a), Initial results from the MAVEN mission to Mars, *Geophys. Res. Lett.*, *42*, 8791–8802, doi:10.1002/2015GL065271.

Jakosky, B. M., et al. (2015b), The Mars Atmosphere and Volatile Evolution (MAVEN) mission, *Space Sci. Rev.*, *195*, 3–48, doi:10.1007/s11214-015-0139-x.

Kallio, E., and P. Janhunen (2001), Atmospheric effects of proton precipitation in the Martian atmosphere and its connection to the Mars-solar wind interaction, *J. Geophys. Res.*, *106*, 5617–5634, doi:10.1029/2000JA000239.

Krasnopolsky, V. A. (2002), Mars' upper atmosphere and ionosphere at low, medium, and high solar activities: Implications for evolution of water, *J. Geophys. Res.*, *107*, 5128, doi:10.1029/2001JE001809.

Larson, D. E., et al. (2015), The MAVEN solar energetic particle investigation, *Space Sci. Rev.*, *195*, 153–172, doi:10.1007/s11214-015-0218-z.
Lee, C., et al. (2017), MAVEN observations of the solar cycle 24 space weather conditions at Mars, *J. Geophys. Res.*, *122*, doi:10.1002/2016JA023495, in press.
Lillis, R. J., M. O. Fillingim, L. M. Peticolas, D. A. Brain, R. P. Lin, and S. W. Bougher (2009), Nightside ionosphere of Mars: Modeling the effects of crustal magnetic fields and electron pitch angle distributions on electron impact ionization, *J. Geophys. Res.*, *114*, E11009, doi:10.1029/2009JE003379.
Lillis, R. J., M. O. Fillingim, and D. A. Brain (2011), Three-dimensional structure of the Martian nightside ionosphere: Predicted rates of impact ionization from Mars Global Surveyor magnetometer and electron reflectometer measurements of precipitating electrons, *J. Geophys. Res.*, *116*, A12317, doi:10.1029/2011JA016982.
Mahaffy, P. R., M. Benna, M. Elrod, R. V. Yelle, S. W. Bougher, S. W. Stone, and B. M. Jakosky (2015a), Structure and composition of the neutral upper atmosphere of Mars from the MAVEN NGIMS investigation, *Geophys. Res. Lett.*, *42*, 8951–8957, doi:10.1002/2015GL065329.
Mahaffy, P. R., et al. (2015b), The neutral gas and ion mass spectrometer on the Mars atmosphere and volatile evolution mission, *Space. Sci. Rev.*, *195*, 49–73, doi:10.1007/s11214-014-0091-1.
Matta, M., P. Withers, and M. Mendillo (2013), The composition of Mars' topside ionosphere: Effects of hydrogen, *J. Geophys. Res. Space Physics*, *118*, 2681–2693, doi:10.1002/jgra.50104.
Mendillo, M., S. Smith, J. Wroten, H. Rishbeth, and D. Hinson (2003), Simultaneous ionospheric variability on Earth and Mars, *J. Geophys. Res.*, *108*, 1432, doi:10.1029/2003JA009961.
Němec, F., D. D. Morgan, D. A. Gurnett, and F. Duru (2010), Nightside ionosphere of Mars: Radar soundings by the Mars Express spacecraft, *J. Geophys. Res.*, *115*, E12009, doi:10.1029/2010JE003663.
Němec, F., D. D. Morgan, D. A. Gurnett, and D. A. Brain (2011), Areas of enhanced ionization in the deep nightside ionosphere of Mars, *J. Geophys. Res.*, *116*, E06006, doi:10.1029/2011JE003804.
Němec, F., D. D. Morgan, C. Diéval, D. A. Gurnett, and Y. Futaana (2014), Enhanced ionization of the Martian nightside ionosphere during solar energetic particle events, *Geophys. Res. Lett.*, *41*, 793–798, doi:10.1002/2013GL058895.
Safaeinili, A., W. Kofman, J. Mouginot, Y. Gim, A. Herique, A. B. Ivanov, J. J. Plaut, and G. Picardi (2007), Estimation of the total electron content of the Martian ionosphere using radar sounder surface echoes, *Geophys. Res. Lett.*, *34*, L23204, doi:10.1029/2007GL032154.
Schneider, N. M., et al. (2015), Discovery of diffuse aurora on Mars, *Science*, *350*, 313, doi:10.1126/science.aad0313.
Schunk, R. W., and A. F. Nagy (2009), *Ionospheres*, 2nd ed., Cambridge Univ. Press, New York.
Sheel, V., S. A. Haider, P. Withers, K. Kozarev, I. Jun, S. Kang, G. Gronoff, and C. Simon Wedlund (2012), Numerical simulation of the effects of a solar energetic particle event on the ionosphere of Mars, *J. Geophys. Res.*, *117*, A05312, doi:10.1029/2011JA017455.
Verigin, M. I., K. I. Gringauz, N. M. Shutte, S. A. Haider, K. Szego, P. Kiraly, A. F. Nagy, and T. I. Gombosi (1991), On the possible source of the ionization in the nighttime Martian ionosphere: 1. Phobos 2 Harp Electron Spectrometer measurements, *J. Geophys. Res.*, *96*, 19,307–19,313, doi:10.1029/91JA00924.
Withers, P. (2009), A review of observed variability in the dayside ionosphere of Mars, *Adv. Space Res.*, *44*, 277–307, doi:10.1016/j.asr.2009.04.027.
Withers, P., et al. (2012), Observations of the nightside ionosphere of Mars by the Mars Express Radio Science Experiment (MaRS), *J. Geophys, Res.*, *117*, A12307, doi:10.1029/2012JA018185.
Withers, P., M. Vogt, P. Mahaffy, M. Benna, M. Elrod, and B. Jakosky (2015), Changes in the thermosphere and ionosphere of Mars from Viking to MAVEN, *Geophys. Res. Lett.*, *42*, 9071–9079, doi:10.1002/2015GL065985.
Xu, S., D. Mitchell, C. Dong, S. Bougher, M. Fillingim, R. Lillis, J. McFadden, C. Mazelle, J. Connerney, and B. Jakosky (2016), Deep nightside photoelectron observations by MAVEN SWEA: Implications for Martian Northern Hemispheric magnetic topology and nightside ionosphere source, *Geophys. Res. Lett.*, *43*, 8876–8884, doi:10.1002/2016GL070527.
Zhang, M. H. G., J. G. Luhmann, and A. J. Kliore (1990), An observational study of the nightside ionospheres of Mars and Venus with radio occultation methods, *J. Geophys. Res.*, *95*, 17,095–17,102, doi:10.1029/JA095iA10p17095.